

- deleterious bacteria in the plant rhizosphere. These mechanisms allow increased plant growth only in native soils, not in sterilized sand cultures such as we have used [J. E. Loper and M. N. Shroth, in *Iron, Siderophores, and Plant Diseases*, T. R. Swinburne, Ed. (Plenum, New York, 1986), pp. 85–98.] Also, some microorganisms have the capability to enhance plant growth by increasing the availability of minerals by increased mineralization processes in native soils. Such a mechanism is ruled out for this system because the effects in our system are specific to the delivery of the toxin and because the plants were provided with an ample amount of available minerals when grown in sand culture [E. A. Curl and B. Truelove, *The Rhizosphere* (Springer-Verlag, Berlin, 1986), pp. 167–176].
- G. B. Lucas, in *Diseases of Tobacco* (Biological Consulting Associates, Raleigh, NC, 1975), pp. 397–409.
  - W. D. Valleau, E. M. Johnson, S. Diachun, *Science* **96**, 164 (1942); *Phytopathology* **34**, 163 (1944).
  - T. J. Knight, R. D. Durbin, P. J. Langston-Unkefer, *Plant Physiol.* **82**, 1045 (1986).
  - P. J. Langston-Unkefer, A. C. Robinson, T. J. Knight, R. D. Durbin, *J. Biol. Chem.* **262**, 1608 (1987).
  - S. L. Sinden and R. D. Durbin, *Nature* **219**, 379 (1968).
  - J. G. Turner, *Physiol. Plant Pathol.* **19**, 57 (1981).
  - J. E. Beringer, N. J. Brown, A. W. B. Johnston, H. M. Schluman, D. A. Hopwood, *Proc. R. Soc. London B204*, 219 (1979) and references therein.
  - M. J. Boland, K. J. F. Farnen, J. G. Robertson, in *Nitrogen Fixation*, W. E. Newton and W. H. Orme-Johnson, Eds. (University Park Press, Baltimore, 1980), pp. 33–52.
  - D. P. S. Verma and S. R. Long, in *Intracellular Symbioses*, K. Jeon, Ed. (Academic Press, New York, 1983), pp. 211–245; D. P. S. Verma and K. Nadler, in *Plant Gene Research: Genes Involved in Plant-Microbe Interactions*, D. P. S. Verma and Th. Hohn, Eds. (Springer-Verlag, New York, 1984), pp. 57–93; S. R. Long, in *Plant-Microbe Interactions: Molecular and Genetic Perspectives*, T. Kosuge and E. W. Nester, Eds. (Macmillan, New York, 1984), pp. 265–306.
  - T. A. Frantz, D. M. Peterson, R. D. Durbin, *Plant Physiol.* **69**, 345 (1982).
  - A. Meister, in *Glutamine: Metabolism, Enzymology, and Regulation*, J. Mora and R. Palacios, Eds. (Academic Press, New York, 1980), pp. 1–40.
  - M. Lara et al., *Planta* **157**, 254 (1983); J. V. Cullimore et al., *J. Mol. Appl. Genet.* **2**, 589 (1984); C. Sengupta-Gopalan and J. W. Pitas, *Plant Mol. Biol.* **7**, 189 (1986).
  - T. J. Knight, R. D. Durbin, P. J. Langston-Unkefer, *J. Bacteriol.* **169**, 1954 (1987).
  - A. Oaks and B. Hirel, *Annu. Rev. Plant Physiol.* **36**, 345 (1985); D. B. Scott, K. J. F. Farnen, J. G. Robertson, *Nature* **263**, 703 (1976).
  - F. O'Gara and K. T. Shanmugam, *Biochim. Biophys. Acta* **437**, 313 (1976).
  - M. L. Kahn, J. Kraus, J. E. Somerville, in *Nitrogen Fixation Research Progress*, H. J. Evans, P. J. Bottomley, W. E. Newton, Eds. (Nijhoff, Dordrecht, 1985), pp. 193–200.
  - D. H. Kohl, K. R. Schubert, M. B. Carter, C. H. Hagedorn, G. Shearer, *Proc. Natl. Acad. Sci. U.S.A.* **85**, 2036 (1988).
  - F. M. Ausubel et al., *J. Bacteriol.* **140**, 597 (1979); K. T. Shanmugam and C. Morandi, *Biochim. Biophys. Acta* **437**, 322 (1976); G. N. Gussin, C. W. Ronson, F. M. Ausubel, *Annu. Rev. Genet.* **20**, 567 (1986).
  - W. W. Szeto, B. T. Nixon, C. W. Ronson, F. M. Ausubel, *J. Bacteriol.* **169**, 1423 (1987); W. W. Szeto, J. L. Zimmerman, V. Sundaresan, F. M. Ausubel, in *Molecular Biology of Development*, E. H. Davidson and R. A. Firtel, Eds. (Liss, New York, 1984), pp. 611–617; C. W. Ronson, B. T. Nixon, L. M. Albright, F. M. Ausubel, *J. Bacteriol.* **169**, 2424 (1987); F. M. Ausubel, *Cell* **37**, 4 (1984).
  - The  $Tox^-$  experiments included the use of four separate spontaneous mutants of *P. syringae* pv. *tabaci* (Pr13) and *P. syringae* pv. *tabaci* ( $Tox^-$ ) (Pa45), a naturally occurring  $Tox^-$  strain. The data are representative of the experiments and are for one of the four spontaneous mutants isolated in our laboratory.
  - R. W. F. Hardy, R. D. Holsten, E. K. Jackson, R. C. Burns, *Plant Physiol.* **43**, 1185 (1968).
  - D. M. Shapiro and E. R. Stadtmann, *Methods Enzymol.* **17A**, 910 (1970).
  - D. A. Cataldo, L. E. Schrader, V. L. Youngs, *Crop Sci.* **14**, 854 (1974).
  - J. V. Cullimore, M. Lara, P. J. Lea, B. J. Milfin, *Planta* **157**, 245 (1983).
  - D. R. Bush and P. J. Langston-Unkefer, *Plant Physiol.* **85**, 845 (1987).
  - This work was supported by the Southwest Consortium on Plant Genetics and Water Relations and was done under the auspices of the U.S. Department of Energy.

29 February 1988; accepted 14 June 1988

## The Incommensurate Modulation of the 2212 Bi-Sr-Ca-Cu-O Superconductor

YAN GAO, PETER LEE, PHILIP COPPENS,\* M. A. SUBRAMANIAN, A. W. SLEIGHT

The incommensurate modulation evident in the diffraction pattern of the superconductor  $Bi_2Sr_{3-x}Ca_xCu_2O_{8+y}$  consists of almost sinusoidally varying displacements of up to 0.4 Å of the Bi and Sr atoms in the  $a$ - and  $c$ -directions of the unit cell, and of up to 0.3 Å of the Cu atoms in the  $c$  direction only. Thus, a newly discovered feature of the  $Bi_2Sr_{3-x}Ca_xCu_2O_{8+y}$  structure is sizable Cu displacement, which is related to static wave formation in the Cu-O sheets. Reported thermal parameters give evidence that similar distortions occur on cooling of the thallium-containing superconductors.

THE CRYSTALLOGRAPHY OF THE 2212 phase of the Bi-Sr-Ca-Cu-O system, with stoichiometry  $Bi_2Sr_{3-x}Ca_xCu_2O_{8+y}$  has been described in a number of publications (1–4). A major feature of the diffraction pattern is the occurrence of satellite reflections, at positions displaced from the main diffraction spots by  $q = \pm 0.21a^*$ , where  $a^*$  is the reciprocal lattice constant. The satellite reflections indicate either a displacive or a substitutional modulation in which position or chemical occupancy vary between unit cells along the  $a$ -axis. Since  $1/q$  is not a simple multiple of  $a$ , the modulation is incommensurate, and the structure cannot be described on a unit cell that is a multiple of the basic cell. Using recently developed methods (5), we have made the first analysis based on the superspace group description of modulated crystals (6).

The room-temperature analysis was performed on two single crystals of different origin and slightly differing cell dimensions. Since the results were essentially identical for the two crystals, only one set is reported here. Crystallographic information is summarized in Table 1. The basic space group is  $Amaa$ , which is a subgroup of space groups reported elsewhere (2–4), but in agreement with at least one earlier study (1). Atomic parameters, obtained in the refinement of

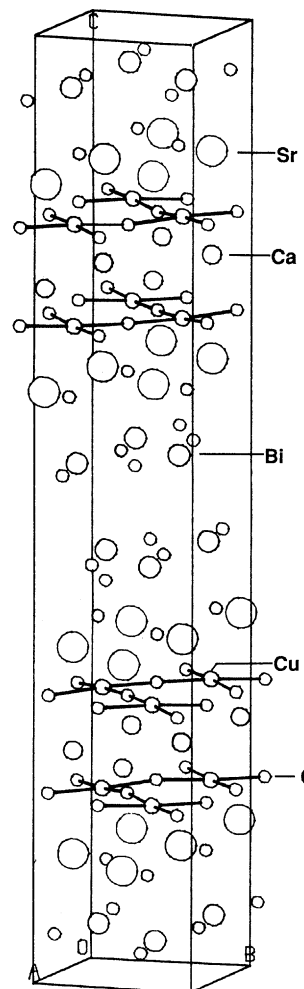


Fig. 1. Packing diagram. The large circles represent Sr atoms; successively smaller circles indicate the Bi, Ca, Cu, and O atoms.

Y. Gao, P. Lee, P. Coppens, Department of Chemistry and Institute on Superconductivity, State University of New York at Buffalo, Buffalo, NY 14214. M. A. Subramanian and A. W. Sleight, Central Research and Development Department, E. I. du Pont de Nemours & Company, Experimental Station, Wilmington, DE 19898.

\*To whom correspondence should be addressed.

**Table 1.** Crystallographic data for single crystal of 2212 phase. Numbers in parentheses are last-digit uncertainties.

<i>a</i>	5.408(1) Å
<i>b</i>	5.413(1) Å
<i>c</i>	30.871(5) Å
<i>V</i>	903.68 Å <sup>3</sup>
<i>Z</i>	4
Space group	M: A <sub>2</sub> ma: $\bar{1}11$
<i>V<sub>c</sub></i>	0.073 × 10 <sup>-3</sup> mm <sup>3</sup>

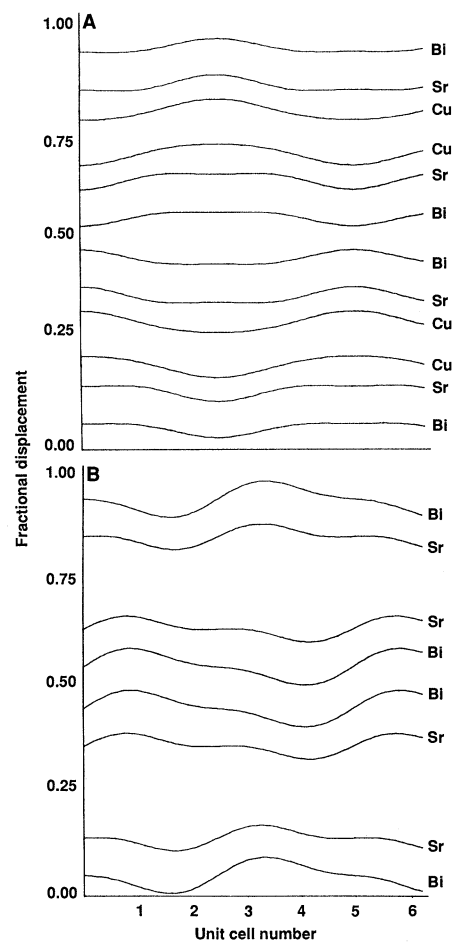


**Fig. 2.** Modulation displacements for successive layers in the crystal on a relative scale. Absolute values are given in Table 3. The horizontal axis is the unit cell number along the crystal *a*-axis. The vertical position of each curve represents the position of the layer on the *c*-axis. (A) Displacements of atoms in the *c* direction. (B) Displacements of atoms in the *a* direction. (Note that the longitudinal displacements along *a* are represented by transverse displacements.)

409 main and 188 first-order satellite reflections, are listed in Table 2. The *R*-factor for the main reflections is 10.75%, whereas the value for the satellites is 15.45%. The structure consists of a series of layers perpendicular to the *c*-axis, including four covalently bonded Cu-O layers per unit cell. A mixed Sr/Ca layer is sandwiched between each pair of Cu-O layers (Fig. 1). The four-dimensional superspace group, based on the diffraction conditions  $k + l + m = 2n$ , and  $h0l$ ,  $h = 2n$  for all  $m$ , where  $m$  is the satellite index, is  $M_{\bar{1}11}^{A_{2}ma}$ . Analysis of the intensities of the satellite reflections shows the major modulation to be displacive rather than substitutional, though a small substitutional component cannot be ruled out. Both first and second harmonic displacement waves exist with phase restrictions as dictated by the space-group symmetry (7). Because the contribution of the oxygen atoms to the scattering is relatively minor their modulation could not be included in the refinement. No modulations were observed for the mixed Sr/Ca layers.

Modulation amplitudes are listed in Table 3. The results are in full agreement with those obtained with the second crystal. For the Bi atom a large modulation in the *a* direction is observed, with a smaller amplitude along *c*. For Sr both amplitudes are of equal magnitude, whereas for the Cu atoms the displacements are only along *c*, in agreement with the strong covalent bonding in the Cu-O planes perpendicular to the *c*-axis. The displacements along the *b* direction are negligible and within experimental errors in all cases. The relative phase of the *a* and *c* displacements of different layers in the crystal is illustrated in Fig. 2. For atoms differing by 1/2 in  $\gamma$  the *c*-axis displacements are the same, but the *a*-axis displacements are inverted. The bunching of Bi atoms observed in the electron micrographs of the [110] projection (8) is likely related to this difference in phase of the *a*-axis displacement of Bi atoms close to  $\gamma = 0.25$  and  $\gamma = 0.75$ . Bi layers near  $z = 0$  and  $z = 1/2$  differ in phase by 180° as observed in the electron micrographs.

The most important result of this study is the large displacement of the Cu atoms,

which has not been previously recognized. The modulation amplitudes of the oxygen atoms cannot be determined from the x-ray data, and no crystal large enough for measurement of a significant number of satellite reflections by neutron diffraction is available at this time. Nevertheless, the change in the positions of the copper atoms implies that present values of the Cu-O-Cu angles may have to be revised. These angles are of importance in determining the strength of the antiferromagnetic superexchange coupling between the Cu (*d*<sup>9</sup>) electrons, which has been invoked in some explanations of the superconducting mechanism. A decrease in this angle reduces the coupling and would increase the transition temperature *T<sub>c</sub>* (9).

Our results indicate a pronounced difference in structure along the *a* and *b* directions. In general displacive modulations are associated with the condensation of soft modes in the crystal. Such modes are clearly important here but do not involve a *b*-axis amplitude.

Published thermal parameters show large apparent vibrational displacements of the Tl, Cu(2), and Ca atoms in the thallium-based high *T<sub>c</sub>* superconductors (10, 11). Such large thermal parameters are typical for a soft mode, which may condense into a static distortion at a lower temperature, leading to a structural modulation. An incipient modulation has been observed in long-exposure electron diffraction patterns of Tl<sub>2</sub>Ba<sub>2</sub>CaCu<sub>2</sub>O<sub>8</sub> (12). Thus, structural modulations of the type studied here appear relatively common in the Cu-O based superconductors.

As there have been reports on Sr deficiency in this material (13), a number of additional refinements were performed varying the Sr occupancy in both the Sr and the Sr/Ca layers. These refinements did not lead to a lowering of the agreement indices. However, a small improvement (to *R* = 10.59% and 15.43% for the main and satellite reflections, respectively) was obtained when the Bi occupancy was varied in addition to the Sr occupancy of the pure strontium layers. The final occupancies [Bi = 0.90(2), Sr = 0.94(4)] indicate a possible Bi deficiency, or substitution of lighter atoms in the Bi layer. The displace-

**Table 2.** Atomic parameters and temperature factors. Numbers in parentheses are last-digit uncertainties (values of *V<sub>ij</sub>* have been multiplied by 10<sup>3</sup>).

Atom	<i>x</i>	$\gamma$	<i>z</i>	<i>U</i> <sub>11</sub> / <i>B</i> <sub>iso</sub>	<i>U</i> <sub>22</sub>	<i>U</i> <sub>33</sub>	<i>U</i> <sub>12</sub>	<i>U</i> <sub>13</sub>	<i>U</i> <sub>23</sub>
Bi	0.50	0.2285(5)	0.0522(1)	27(2)	17(1)	8(2)	0	0	2(2)
Sr	0.00	0.2537(10)	0.1409(2)	10(4)	6(4)	15(4)	0	0	-0(5)
Cu	0.50	0.2498(13)	0.1967(3)	4(3)	2(5)	20(5)	0	0	-2(6)
Ca/Sr	0.50	0.25	0.25	7(6)	7(5)	71(11)	0	0	-0(7)
O(1)	0.75	0.00	0.195(2)	1.7(10)					
O(2)	0.25	0.50	0.202(2)	1.5(10)					
O(3)	0.50	0.28(1)	0.122(2)	4.9(15)					
O(4)	0.00	0.15(2)	0.053(4)	10.1(28)					

**Table 3.** Atomic displacement amplitudes (Å). Numbers in parentheses are last-digit uncertainties.

Atom	Direction	Phase	Amplitude	
			First harmonic	Second harmonic
Bi	<i>u</i> (a)	0	-0.39(1)	0.15(1)
	<i>u</i> (b)	90	0.04(1)	-0.02(2)
	<i>u</i> (c)	90	0.19(1)	-0.06(1)
Sr	<i>u</i> (a)	0	-0.24(1)	0.15(2)
	<i>u</i> (b)	90	-0.03(3)	-0.05(6)
	<i>u</i> (c)	90	0.20(1)	-0.08(2)
Cu	<i>u</i> (a)	0	-0.04(1)	0.04(4)
	<i>u</i> (b)	90	0.00(3)	0.04(10)
	<i>u</i> (c)	90	0.28(1)	-0.04(2)

ment amplitudes reported in Table 3 were not significantly altered in these refinements.

#### REFERENCES AND NOTES

1. M. A. Subramanian *et al.*, *Science* **239**, 1015 (1988).
2. P. Bordet *et al.*, in *Proceedings of the International Conference on High Temperature Superconductors and Materials and Mechanisms of Superconductivity*, J. Müller and J. L. Olsen, Eds. (North-Holland, Amsterdam, 1988), pp. 623–624.
3. S. A. Sunshine *et al.*, *Phys. Rev. Sect. B* **38**, 893 (1988).
4. J. M. Tarascon *et al.*, *ibid.* **37**, 9382 (1988).
5. V. Petricek, P. Coppens, P. Becker, *Acta Crystallogr. Sect. A* **41**, 478 (1985).
6. P. M. De Wolff, T. Janssen, A. Janner, *ibid.* **37**, 625 (1981).
7. V. Petricek and P. Coppens, *Acta Crystallogr. Sect. A.*, in press.
8. T. M. Shaw *et al.*, *Phys. Rev. B* **37**, 9856 (1988); P. L. Gai and P. Day, *Physica C*, in press.
9. G. Chen and W. A. Goddard III, *Science* **239**, 899 (1988).
10. C. C. Torardi *et al.*, *ibid.* **240**, 631 (1988).
11. M. A. Subramanian *et al.*, *Nature* **332**, 420 (1988).
12. J. D. Fitzgerald *et al.*, *Phys. Rev. Lett.* **60**, 2797 (1988).
13. A. K. Cheetham, A. M. Chippindale, S. J. Hibble, *Nature* **333**, 21 (1988); A. M. Chippindale *et al.*, *Physica C* **152**, 154 (1988).
14. Support of this work by the National Science Foundation (CHE8711736) is gratefully acknowledged.

22 June 1988; accepted 19 July 1988

## Neutron Imaging of Laser Fusion Targets

D. RESS, R. A. LERCHE, R. J. ELLIS, S. M. LANE, K. A. NUGENT

**A long-term goal of inertial-confinement fusion research is the generation of energy by imploding capsules containing deuterium-tritium fuel. Progress in designing the capsules is aided by accurate imaging of the fusion burn. Penumbra coded-aperture techniques have been used to obtain neutron images that are a direct measurement of the fusion burn region in the capsules.**

NEUTRON IMAGES OF LASER-DRIVEN inertial confinement fusion (ICF) targets were recently obtained at the Nova laser facility of the Lawrence Livermore National Laboratory (LLNL). These images provide a direct measurement of the deuterium-tritium (DT) fusion burn region within a compressed target. We describe the imaging system, review the physics of neutron emission by ICF implosions, present two examples of the neutron images, and compare the experimental results with theoretical predictions.

A major goal of ICF research is the generation of energy by imploding targets containing DT fuel. Efficient energy production requires that such a target produce 100 times more energy than is used to drive the implosion. This high gain can be obtained by compressing the fuel in a particular fashion (1). Most of the fuel is strongly com-

pressed to a density  $\rho > 200 \text{ g/cm}^3$  at the relatively low ion temperature  $\theta_i \approx 1 \text{ keV}$ . At the center of this highly compressed fuel is a much smaller "hot spot" containing about 1% of the fuel mass at a much lower density ( $\rho > 30 \text{ g/cm}^3$ ) but higher temperature ( $\theta_i \approx 4 \text{ keV}$ ). Fusion is initiated in this hot spot, producing a thermonuclear burn wave that propagates into the surrounding cooler fuel.

Previous diagnostic techniques do not diagnose hot-spot formation and ignition. X-ray emission, which is the basis for many widely used ICF diagnostics, depends on the spatial and temporal profiles of the plasma density, ionization state, and electron temperature. During an ICF implosion, the electron and ion temperatures can be quite different, and mixing of target components leads to complicated spatial variations in the ionization state. Thus, an x-ray image provides information about the spatial structure of several complex processes within the target that are not directly related to the fusion reaction. A neutron image, on the other hand, provides a direct measurement of the spatial extent of the fusion reaction. Fur-

thermore, in advanced targets that achieve high compression, most reaction products and x-rays are absorbed within the target; only the neutrons escape. Neutron imaging, therefore, has long been recognized for its potential to unambiguously diagnose both compression and hot-spot formation in the burning fuel (2).

ICF experiments at Nova will soon focus on the physics of hot-spot formation. Because of the limited energy of the Nova laser, these experiments will create implosions that contain only the hot-spot region and do not ignite. For such targets, the neutron emission region is less than  $25 \mu\text{m}$  in diameter with a yield (neutrons produced per implosion) of  $10^{11}$ . Conventional pinhole imaging is not sensitive enough to produce neutron images of such targets. Penumbra imaging, a technique previously used to obtain x-ray images of laser-produced plasmas (3), has been suggested as a more efficient method to image neutrons emitted by ICF targets (4). Our recent numerical and theoretical calculations verified the feasibility of neutron penumbra imaging. Here we report experimental results obtained with a preliminary neutron imaging system for ICF.

Penumbra imaging is a coded-aperture-imaging technique. It is conceptually similar to pinhole imaging with the essential difference that the aperture is larger than the source. The geometry of penumbra imaging is shown in Fig. 1. The image produced consists of a uniform bright region surrounded by a partially illuminated penumbra. All the spatial information about the source is encoded in this penumbra.

The neutron penumbra imaging system

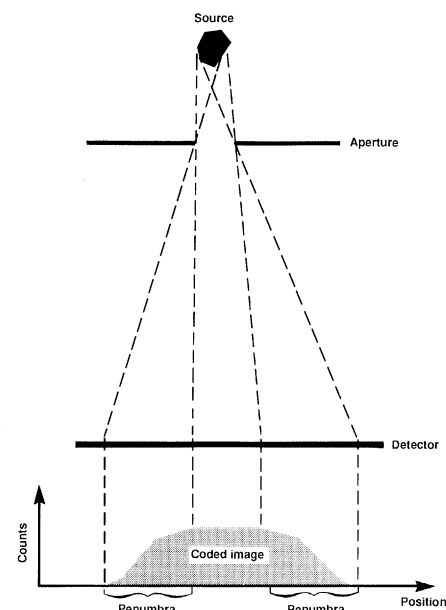


**Fig. 1.** Geometry of the penumbra imaging process.

D. Ress, R. A. Lerche, R. J. Ellis, S. M. Lane, Lawrence Livermore National Laboratory, P.O. Box 808, Livermore, CA 94550.  
K. A. Nugent, The University of Melbourne, School of Physics, Parkville, Victoria, Australia 3052.